

Coupling interlayer excitons to whispering gallery modes in van der Waals heterostructures

Ronja Khelifa,¹ Patrick Back,¹ Nikolaus Flöry,¹ Shadi Nashashibi,^{1,2} Konstantin Malchow,^{1,3} Takashi Taniguchi,⁴ Kenji Watanabe,⁵ Achint Jain,¹ and Lukas Novotny¹

¹*Photonics Laboratory, ETH Zürich, 8093 Zürich, Switzerland*

²*Present address: Institute of Electromagnetic Fields, ETH Zürich, 8092 Zürich, Switzerland*

³*Present address: Laboratoire Interdisciplinaire Carnot de Bourgogne, UMR 6303 CNRS-Université de Bourgogne Franche-Comté, 21078 Dijon, France*

⁴*International Center for Materials Nanoarchitectonics,*

National Institute for Materials Science, 1-1 Namiki, Tsukuba 305-0044, Japan

⁵*Research Center for Functional Materials, National Institute for Materials Science, 1-1 Namiki, Tsukuba 305-0044, Japan*

(Dated: July 10, 2020)

Van der Waals heterostructures assembled from two-dimensional materials offer a promising platform to engineer structures with desired optoelectronic characteristics. Here we use waveguide-coupled disk resonators made of hexagonal boron nitride (h-BN) to demonstrate cavity-coupled emission from interlayer excitons of a heterobilayer of two monolayer transition metal dichalcogenides. We sandwich a MoSe₂ – WSe₂ heterobilayer between two slabs of h-BN and directly pattern the resulting stack into waveguide-coupled disk resonators. This enables us to position the active materials into regions of highest optical field intensity, thereby maximizing the mode overlap and the coupling strength. Since the interlayer exciton emission energy is lower than the optical band gaps of the individual monolayers and since the interlayer transition itself has a weak oscillator strength, the circulating light is only weakly reabsorbed, which results in an unaffected quality factor. Our devices are fully waveguide-coupled and represent a promising platform for on-chip van der Waals photonics.

Keywords: interlayer excitons, transition metal dichalcogenides, h-BN photonics, whispering gallery mode resonator

Van der Waals (vdW) heterostructures made of a vertical assembly of two-dimensional (2D) materials like transition metal dichalcogenides (TMDCs) and graphene have opened up new possibilities for optoelectronic devices [1, 2]. Since adjacent 2D materials are held together by weak van der Waals forces, they can be stacked without need of lattice matching and can be placed on almost any substrate [3, 4]. In their monolayer form, TMDCs exhibit a direct bandgap [5, 6], which makes them excellent candidates for optoelectronic devices as well as for integration with optical cavities for enhanced light-matter interactions [7–12].

By combining two dissimilar TMDC monolayers into a heterobilayer (HBL), interlayer excitons with spatially separated electrons and holes can be formed [13]. Their charge carrier dynamics [14], electrically tunable exciton resonances [13, 15] and the possibility of creating p-n junctions [16], are providing intriguing possibilities for materials engineering. Recently, motivated by a growing interest in nanolasers, interlayer excitons were coupled to silicon-based photonic crystals [17], as well as grating cavities [18], to realize surface-emitting, optically pumped lasers at room-temperature.

However, the co-integration of light-emitting devices (LEDs) and lasers made of vdW heterostructures with on-chip photonic structures, such as waveguides and resonators, requires in-plane light guiding. Coupling via evanescent fields has been achieved, for example, by placing vdW materials on top of silicon-based waveguides [1, 2] and ring resonators [19], but the coupling strength

obtainable in this manner is modest because the highest field intensity is found inside the light-confining dielectric medium. Optimal mode overlap can be achieved by integrating the active layer into dielectric waveguides or resonators. For optically excited systems, this has been shown by sandwiching a monolayer WS₂ into a microdisk made of Si₃N₄/hydrogen silsesquioxane (HSQ) [8] or hexagonal boron nitride (h-BN) [20]. However, in both of these structures the disk was freestanding and is not easily compatible with on-chip photonics.

Here we present vdW heterostructures patterned into waveguide-coupled disk resonators, as illustrated in Fig. 1a. The stacking allows us to place TMDCs into regions of high field intensity. Our approach combines two important attributes: 1) an enhanced optical mode overlap and 2) waveguide coupling for on-chip integration. These are enabling factors for the development of on-chip optoelectronic devices, such as LEDs, modulators and photodetectors. For the dielectric material we chose h-BN, which has already been used to fabricate photonic structures like resonators or photonic crystals [20–22] and has been proposed as a confinement layer in integrated photonics [23]. In addition to its favorable photonic attributes, h-BN also provides a means of encapsulation, that is, by placing TMDCs in between h-BN we prevent them from degradation [24].

As shown in Fig. 1a, we integrate a HBL into an h-BN disk resonator, which can be excited by laser light propagating along a nearby waveguide. Photoluminescence (PL) associated with the interlayer exciton is coupled

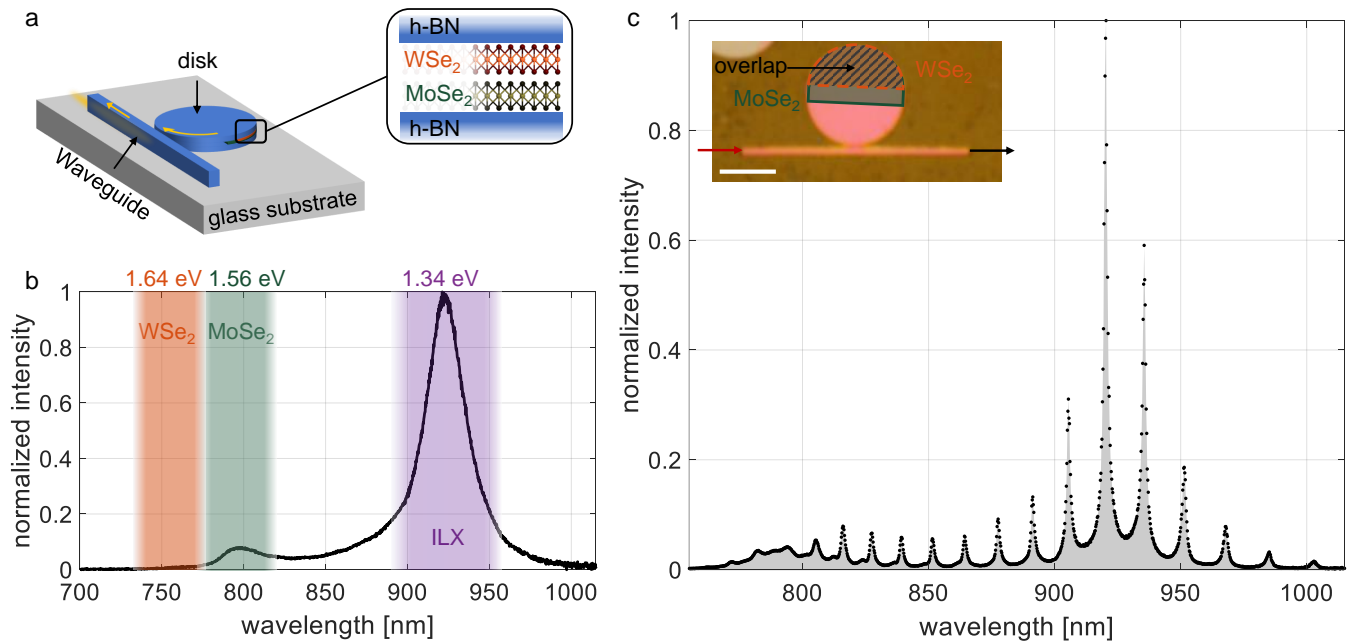


FIG. 1. (a) Illustration of a waveguide-coupled disk resonator with integrated heterobilayer (HBL). The HBL is sandwiched between two h-BN flakes. The emission from the interlayer exciton is coupled to whispering gallery modes (WGM) of the disk resonator and then outcoupled through the same waveguide used for excitation. (b) Free-space photoluminescence (PL) spectrum of the HBL, showing strong emission from the interlayer exciton (ILX) and quenched intralayer exciton emission. (c) Cavity-coupled photoluminescence spectrum featuring distinct peaks separated by the free-spectral range of the WGMs of the disk resonator. The resonator is excited at $\lambda = 633$ nm from one end of the waveguide and the photoluminescence is detected at the other end. The intralayer exciton emission is strongly suppressed because of reabsorption. The scale bar is $5 \mu\text{m}$.

out by the adjacent waveguide. The unique feature of our approach is that both, the active material (TMDCs) as well as the dielectric (h-BN) are assembled into a single vdW heterostructure and subsequently patterned into the final photonic circuit (disk resonator and waveguide). This differs from previous works [1, 2, 19], where TMDCs were transferred on top of pre-fabricated photonic elements. As illustrated in Fig. 1b, the interlayer exciton emission energy is lower than the optical band gaps of the individual monolayers, which leads to weak reabsorption of the interlayer emission. Reabsorption is further suppressed by the weak oscillator strength of the direct interlayer exciton transition [16, 25]. As a result, the quality (Q)-factor of the coupled mode is largely unaffected by reabsorption. Figure 1c shows the spectrum of the waveguide-coupled interlayer emission. The vdW disk has been excited from one end of the waveguide with a 633 nm laser and the PL has been detected at the other end. In the following we first describe the fabrication procedure, then present the characteristics of the HBL and h-BN disks and finally discuss the results of the combined system.

Flakes of h-BN and monolayers of WSe₂ and MoSe₂ were prepared by mechanical exfoliation and assembled into vdW heterostructures using a polymer-based stacking technique [26, 27]. The crystallographic axes of the two monolayers were rotationally aligned. Atomic force

microscopy was utilized to identify h-BN flakes of the desired thicknesses. Figures 2b and c (magnified) show optical microscope images of such an h-BN – MoSe₂ – WSe₂ – h-BN heterostructure on a glass substrate. As illustrated in Fig. 2a, waveguides and disk resonators were fabricated from the vdW stack using electron-beam lithography and reactive ion etching with aluminum as a hard mask. Fig. 2d shows the final device. The disk resonator has a total thickness of ~ 310 nm and a design radius of $4.25 \mu\text{m}$. A more detailed description of the fabrication procedure can be found in the methods section in the Supporting Information (SI).

In order to determine the emission energies we performed PL measurements of the TMDC monolayers and of the HBL region using a 633 nm continuous wave (cw) He-Ne laser. The PL spectra of the individual monolayers reveal direct intralayer exciton emission peaks at 755 nm (1.64 eV) and 793 nm (1.56 eV) for WSe₂ and MoSe₂, respectively, and are in agreement with previous works [14, 17, 28, 29] (details in the SI). In Fig. 1b we show the PL spectrum of the HBL, with a pronounced peak at around 923 nm (1.34 eV). This feature is identified as the interlayer exciton emission and can be explained by the type-II band alignment of MoSe₂ and WSe₂ in the overlap region [13, 18]. In this process the absorption of a photon in a monolayer is followed by a charge transfer to the energetically favorable band of the neighboring monolayer,

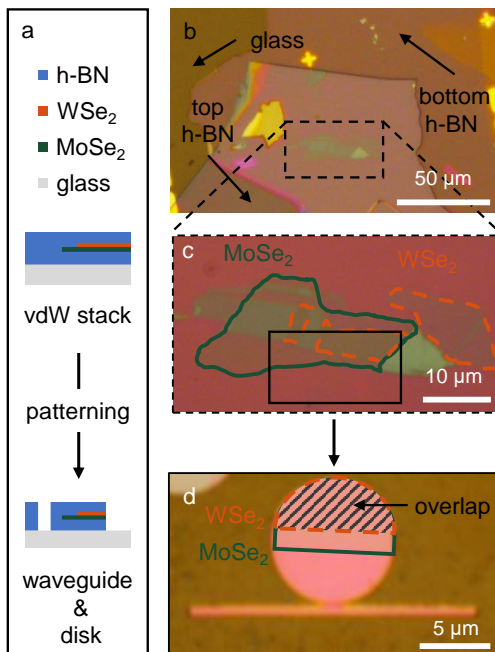


FIG. 2. (a) Schematic of the fabrication procedure, showing cross-sections of the van der Waals (vdW) heterostructure after stacking and after subsequent patterning into a waveguide-coupled disk resonator (not to scale). (b,c) Optical microscope images of the h-BN – MoSe₂ – WSe₂ – h-BN heterostructure after stacking. The heterostructure has a total thickness of ~ 310 nm (bottom h-BN: ~ 150 nm and top h-BN: ~ 158 nm). (d) Electron-beam lithography and reactive ion etching were utilized to pattern the vdW heterostructure into a waveguide-coupled disk resonator with a design radius of $4.25 \mu\text{m}$

leading to a spatial separation of electron and hole. As a result, a strong decrease of the intralayer exciton emissions can be observed. Furthermore, for two rotationally aligned monolayers the interlayer exciton exhibits a direct band gap character [30]. The strong interlayer peak in combination with the quenching of intralayer exciton emission in Fig. 1b consequently verifies the good electrical coupling and the near perfect rotational alignment of the two layers.

To investigate the properties of h-BN waveguide-coupled disk resonators we fabricated reference structures without integrated TMDCs. Figure 3a shows a typical transmission spectrum of a fabricated device. It was obtained by focusing a broadband supercontinuum laser on one waveguide facet and detecting the transmitted light at the other end of the waveguide. The recorded spectrum features sharp dips at wavelengths that satisfy the resonance conditions of the disk resonator. The envelope of the spectrum is defined by the excitation spectrum and the transmission characteristics of the experiment. The Q-factors of the resonances reach values of ~ 1000 . The spectral positions of the resonance peaks, the Q-factors and the free spectral range depend sensi-

tively on the h-BN thickness and the disk radius (details in the SI). Using finite element simulations as a guide, we define the disk radius for a given stack thickness in order to optimize the resonances for the interlayer emission spectrum (details on simulations in the SI). As shown in Fig. 3c, the computed electric field distribution is highest near the rim of the disks and near the vertical center. Therefore, to optimize the coupling strength to the interlayer exciton the HBL should be sandwiched into the h-BN resonator.

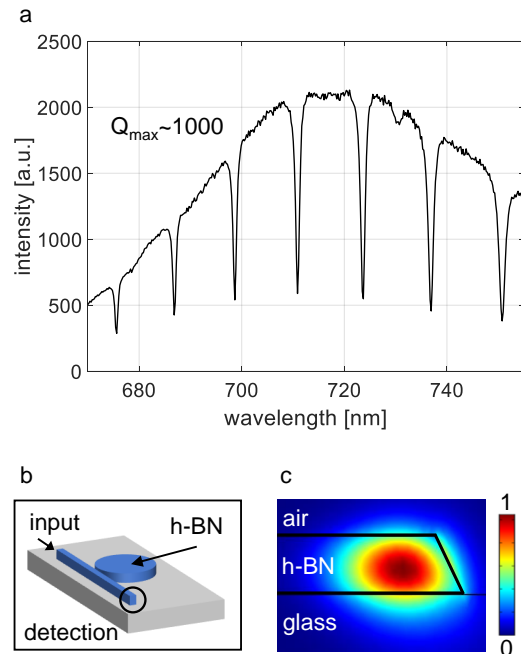


FIG. 3. (a) Transmission spectrum of an h-BN waveguide-coupled disk resonator without integrated TMDC. The dips correspond to the resonances of the WGMs and the envelope is determined by the spectrum of the broadband laser source and the transmission characteristics of the setup and waveguide. (b) Sketch of the h-BN waveguide-coupled disk resonator. (c) Simulated electric field distribution (absolute value) near the rim of a disk resonator (cross-sectional view).

Next, we characterize an h-BN disk resonator with integrated TMDC heterobilayer. We vary the location of the excitation in order to investigate the coupling of the interlayer emission to the WGMs of the disk. As shown in the sketch and the optical microscope image in Figs. 4a and b, coupling to WGMs and interlayer excitons can be achieved by placing the excitation spot near the edge of the disk. We use the same objective for excitation and detection. The emission is detected either at the same position as the excitation spot or at the ends of the waveguide. The light coupled out at the end of the waveguide is partially refracted into the glass substrate and can be captured at high angles with the oil-immersion objective (NA=1.4) that we use. This allows us to compare the spectra of free-space PL (detected at the excitation spot on the disk) and cavity-coupled PL

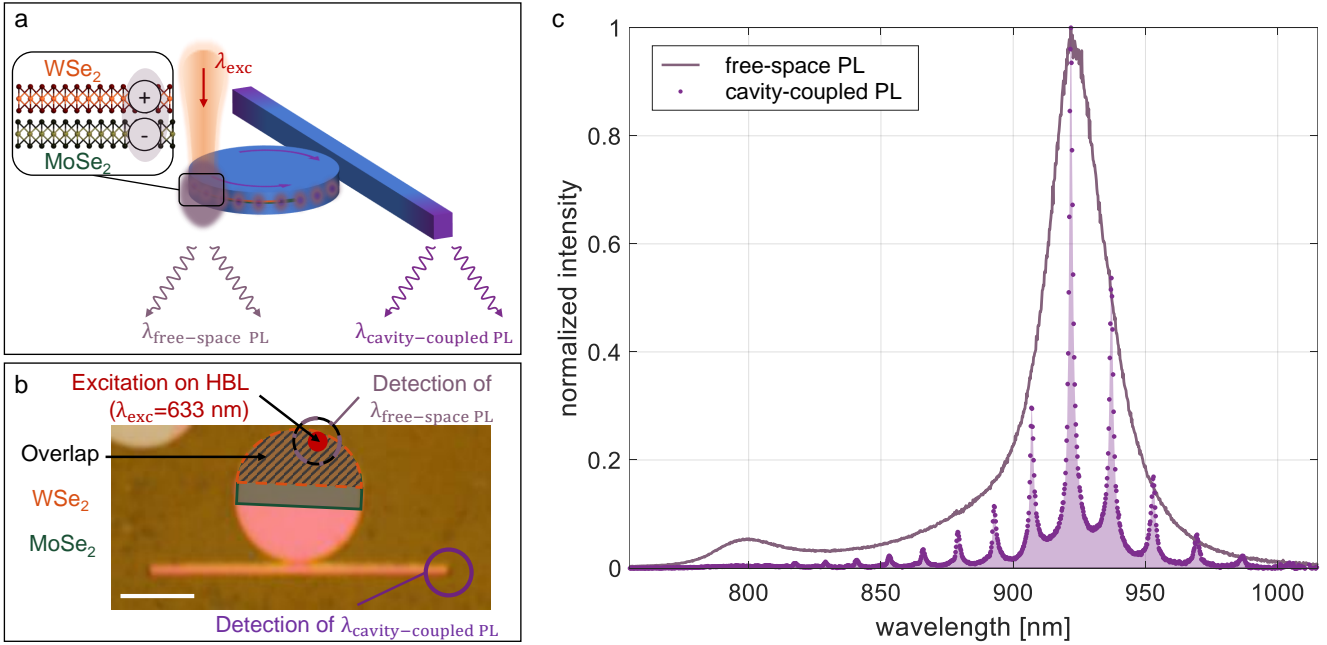


FIG. 4. (a) Illustration of cavity-coupled and free-space detection. Comparison of the spectra recorded by the two detection schemes provides information on reabsorption in the h-BN resonator. (b) Optical microscope image indicating the locations of excitation and detection, and the regions with MoSe₂, WSe₂ and their overlap (HBL region). The structure is excited with a 633 nm cw laser at the edge of the disk, on the HBL region. The scale bar is 5 μm . (c) Measured spectrum at the waveguide end (cavity-coupled PL) and at the excitation spot (free-space PL). Interlayer emission can be detected at the ends of the waveguide. The PL detected at the excitation spot coincides well with the envelope function of the cavity-coupled PL.

(detected at the waveguide end). As shown in Fig. 4c, the spectrum of the free-space PL is in agreement with the expected interlayer emission of the HBL (cf. Fig. 1b). On the other hand, the cavity-coupled spectrum, detected at the waveguide end, exhibits distinct peaks that are separated by the free-spectral range of the WGMs of the disk resonator. We emphasize that, in contrast to several other recent studies [8, 9, 20], the waveguide-coupled spectrum features a reduced background because it is not superimposed to free-space PL.

As shown in the inset of Fig. 5a, the two TMDCs forming the HBL do not overlap over the entire footprint of the disk. There are regions where only the MoSe₂ monolayer can be directly excited. Figure 5a shows the corresponding spectrum of the free-space and cavity-coupled PL. The main contribution of the cavity-coupled PL comes from the intralayer exciton emission of the MoSe₂ monolayer. Interestingly, however, the envelope function of the resonances does not coincide with the free-space PL, measured at the excitation spot. Instead, the highest peak intensity of the cavity-coupled PL is positioned at wavelengths longer than the free-space PL emission peak. We attribute this observation to reabsorption of the emitted PL in the cavity by the MoSe₂ monolayer itself. This interpretation is supported by the absorption spectrum of MoSe₂, visualized by the extinction coefficient, i.e. the imaginary part of the refractive index (taken from [31]), which we include in Fig. 5a (dashed

curve). Thus, the spectral overlap of the cavity-coupled PL with the extinction coefficient causes significant reabsorption for wavelengths in this spectral range. As a result, the corresponding peak intensities of the cavity-coupled PL are reduced for these wavelengths. The peaks at longer wavelengths have an additional contribution from interlayer emission from the HBL. This emission is made possible by the reabsorption of the monolayer emission in the overlap region of the two TMDCs. The effect of enhanced reabsorption in a sandwiched structure is further discussed in the Supporting Information, where two structures with integrated monolayer TMDCs are compared: 1) a sandwiched device and 2) a device with a monolayer transferred on top of the disk. The comparison shows that reabsorption in a sandwiched device is significantly stronger, due to the enhanced mode overlap.

The coupling of interlayer excitons to WGMs, profits not only from the enhanced mode overlap in the sandwiched structure, but also from low intrinsic reabsorption. The latter is due to the low oscillator strength of the interlayer transition, resulting from the spatial separation of the charge carriers [16, 25]. The oscillator strength of the interlayer exciton in MoSe₂ – WSe₂ has been experimentally determined to be two orders of magnitude lower than that of the intralayer exciton [16]. In addition, in differential reflectance measurements, a reduced interlayer exciton absorption has also been shown,

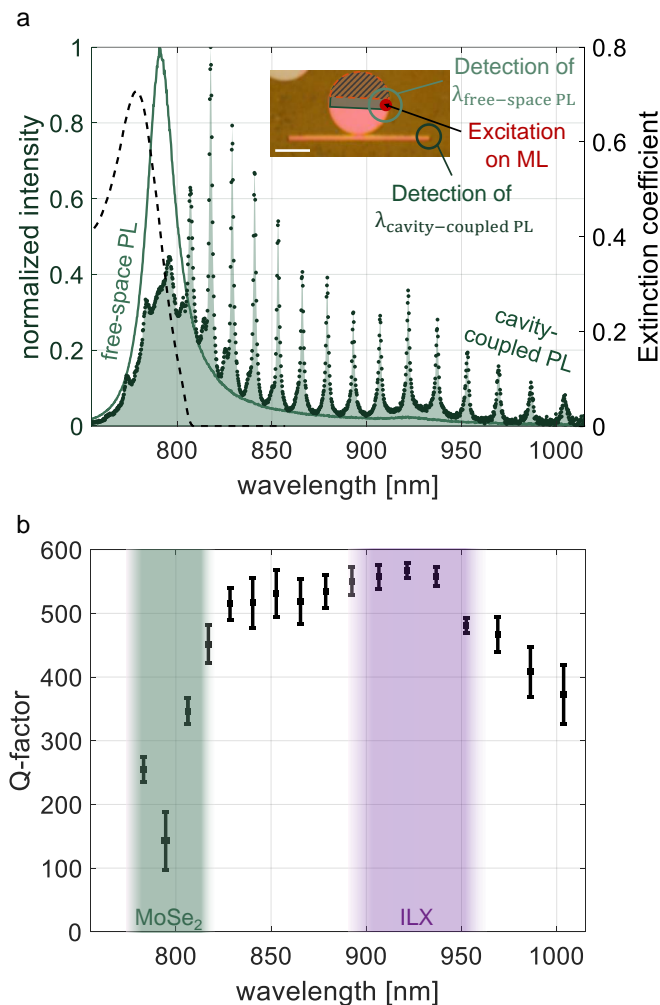


FIG. 5. (a) Measured spectra at the waveguide end (cavity-coupled PL) and at the excitation spot (free-space PL), when exciting at the MoSe₂ monolayer region, as indicated in the inset (scale bar is 5 μm). The envelope function of the cavity-coupled PL does not coincide with the free-space PL. Indicating strong reabsorption of intralayer emission by the MoSe₂ monolayer itself. The dashed curve indicates the MoSe₂ extinction spectrum (taken from [31]). (b) Wavelength dependence of the Q-factor, determined by fitting Lorentzian functions to the measured resonances. Measurements were taken for different locations of excitation (HBL, monolayer, waveguide end) and detection at both waveguide ends. The means and the standard deviations are shown in the figure. A strong drop in Q-factor can be observed at the absorption wavelengths of the intralayer exciton transition of MoSe₂. No drop in Q-factor is observed for wavelengths of the interlayer exciton transition, indicating low reabsorption.

albeit at low-temperatures [25]. This is in agreement with our measurements shown in Fig. 4c, where the HBL has been excited. Here, the free-space PL agrees well with the envelope function of the cavity-coupled resonance peaks. To summarize, our data indicates that the

intralayer emission from monolayer TMDCs is strongly reabsorbed compared to the interlayer emission. The integration of a HBL inside the disk resonator consequently has two benefits: 1) strong absorption of the excitation by intralayer excitons and 2) weak reabsorption of the interlayer emission within the cavity.

To allow for an absolute comparison of intralayer and interlayer coupling to WGMs, we now discuss waveguide-coupled excitation and read-out of the disk resonator (Fig. 1c inset). The data in Fig. 1c shows that the highest peak intensity is observed at wavelengths corresponding to the interlayer emission. In fact, the monolayer emission is strongly suppressed, in agreement with our previous conclusions. We estimate a ratio of ~ 13 between the peak intensities of the main resonances (~ 920 nm and ~ 820 nm) of interlayer and intralayer emission (details in the SI). Note that the spectrum in Fig. 1c has been corrected for the wavelength dependent transmission of our measurement setup and the CCD detection efficiency. Our waveguide-coupled experiments support our previous conclusion that intralayer emission from TMDC monolayers is largely reabsorbed.

As shown in Fig. 5b, the Q-factors of the emission peaks are wavelength dependent, which is a result of the optical properties of the incorporated TMDC HBL. The highest values are ~ 570 and occur at wavelengths that correspond to the interlayer emission peak. In contrast, a considerably lower Q-factor is observed for wavelengths near the optical band gap of MoSe₂. This provides further support for the reabsorption of monolayer emission discussed earlier. Because of the low oscillator strength of the interlayer transition the reabsorption of interlayer emission is significantly weaker, which is evidenced by the high Q-factor at wavelengths near the interlayer transition. The decrease in Q-factor at longer wavelengths (>950 nm) can be explained by radiation losses, which increase at higher wavelengths (see SI). Our Q-factors are currently limited by fabrication imperfections and the h-BN sidewall roughness arising from etching (see scanning electron microscope image in the SI). Nevertheless, even with integrated TMDCs and a coupled waveguide, we achieve Q-factors that are slightly higher than those reported for h-BN ring resonators [22]. Our Q-factors could be increased even further by removing the substrate underneath the outer regions of the disk where the WGMs are localized [8, 20].

In summary, we have demonstrated the coupling of interlayer excitons from a TMDC HBL to WGMs of an h-BN disk resonator. We achieve high coupling strengths by sandwiching the HBL into the h-BN disk. The high oscillator strengths of intralayer transitions of the two monolayers lead to a high absorption efficiency. On the other hand, the low oscillator strength of the interlayer transition suppresses the reabsorption at the emission wavelength. The combination of these two effects gives rise to strong interlayer emission from our vdW disk resonators.

Considering the fact that patterning photonic struc-

tures out of h-BN and vdW heterostructures is still in its infancy, further improvements in performance with optimized fabrication techniques (e.g. optimization of the etching process) is expected. To proceed one step further towards on-chip optoelectronics, light sources need to be co-integrated with photonic structures. The recent progress in electrical control of interlayer excitons [15], as well as the realization of light emitting devices [15, 16, 32], demonstrates a wide range of possibilities for band structure engineering with HBLs. Therefore, combining our approach with electrically tunable interlayer excitons, offers a promising platform for on-chip integrated photonics based on 2D materials.

ACKNOWLEDGMENTS

This work has been supported by the Swiss National Science Foundation (grant 200020_192362/1). The authors thank A. Kuzmina, D. Windey, S. Papadopoulos, R. Reimann, M. Parzefall and S. Heeg for fruitful discussions. In addition the authors thank A. İmamoglu at ETH Zürich for the usage of the stacking setup. The use of the facilities of the FIRST center for micro- and nanoscience at ETH Zürich is gratefully acknowledged. K.W. and T.T. acknowledge support

from the Elemental Strategy Initiative conducted by the MEXT, Japan, Grant Number JPMXP0112101001, JSPS KAKENHI Grant Numbers JP20H00354 and the CREST(JPMJCR15F3), JST.

AUTHOR CONTRIBUTIONS

L.N. and R.K. conceived the project. R.K. and P.B. fabricated the devices and performed the experiments. A.J., N.F. contributed to the experiments. S.N. and K.M. performed preliminary studies. T.T. and K.W. synthesized the h-BN crystals. R.K., P.B., N.F., A.J. and L.N. analysed the data and co-wrote the manuscript.

SUPPORTING INFORMATION

The Supporting Information includes descriptions of: sample fabrication, methods of measurements, photoluminescence measurements, characterization of h-BN disk resonators, simulations of h-BN disk resonators, study of vertical emitter position inside h-BN disk resonator, determination of Q-factor, as well as comparison of the resonance peak intensities for the waveguide-coupled disk resonator with integrated heterobilayer.

-
- [1] Bie, Y. Q.; Grosso, G.; Heuck, M.; Furchi, M. M.; Cao, Y.; Zheng, J.; Bunandar, D.; Navarro-Moratalla, E.; Zhou, L.; Efetov, D. K. et al. A MoTe₂-based light-emitting diode and photodetector for silicon photonic integrated circuits. *Nature Nanotechnology* **2017**, *12*, 1124–1129.
- [2] Flöry, N.; Ma, P.; Salamin, Y.; Emboras, A.; Taniguchi, T.; Watanabe, K.; Leuthold, J.; Novotny, L. Waveguide-integrated van der Waals heterostructure photodetector at telecom wavelengths with high speed and high responsivity. *Nature Nanotechnology* **2020**, *15*, 118–124.
- [3] Geim, A. K.; Grigorieva, I. V. Van der Waals heterostructures. *Nature* **2013**, *499*, 419–425.
- [4] Liu, Y.; Weiss, N. O.; Duan, X.; Cheng, H. C.; Huang, Y.; Duan, X. Van der Waals heterostructures and devices. *Nature Reviews Materials* **2016**, *1*, 16042.
- [5] Splendiani, A.; Sun, L.; Zhang, Y.; Li, T.; Kim, J.; Chim, C. Y.; Galli, G.; Wang, F. Emerging photoluminescence in monolayer MoS₂. *Nano Letters* **2010**, *10*, 1271–1275.
- [6] Mak, K. F.; Lee, C.; Hone, J.; Shan, J.; Heinz, T. F. Atomically thin MoS₂: A new direct-gap semiconductor. *Physical Review Letters* **2010**, *105*, 136805.
- [7] Wu, S.; Buckley, S.; Schaibley, J. R.; Feng, L.; Yan, J.; Mandrus, D. G.; Hatami, F.; Yao, W.; Vučković, J.; Majumdar, A. et al. Monolayer semiconductor nanocavity lasers with ultralow thresholds. *Nature* **2015**, *520*, 69–72.
- [8] Ye, Y.; Wong, Z. J.; Lu, X.; Ni, X.; Zhu, H.; Chen, X.; Wang, Y.; Zhang, X. Monolayer excitonic laser. *Nature Photonics* **2015**, *9*, 733–737.
- [9] Reed, J. C.; Malek, S. C.; Yi, F.; Naylor, C. H.; Charlie Johnson, A. T.; Cubukcu, E. Photothermal characterization of MoS₂ emission coupled to a microdisk cavity. *Applied Physics Letters* **2016**, *109*, 193109.
- [10] Li, Y.; Zhang, J.; Huang, D.; Sun, H.; Fan, F.; Feng, J.; Wang, Z.; Ning, C. Z. Room-temperature continuous-wave lasing from monolayer molybdenum ditelluride integrated with a silicon nanobeam cavity. *Nature Nanotechnology* **2017**, *12*, 987–992.
- [11] Shang, J.; Cong, C.; Wang, Z.; Peimyoo, N.; Wu, L.; Zou, C.; Chen, Y.; Chin, X. Y.; Wang, J.; Soci, C. et al. Room-temperature 2D semiconductor activated vertical-cavity surface-emitting lasers. *Nature Communications* **2017**, *8*, 543.
- [12] Javerzac-Galy, C.; Kumar, A.; Schilling, R. D.; Piro, N.; Khorasani, S.; Barbone, M.; Goykhman, I.; Khurgin, J. B.; Ferrari, A. C.; Kippenberg, T. J. Excitonic Emission of Monolayer Semiconductors Near-Field Coupled to High-Q Microresonators. *Nano Letters* **2018**, *18*, 3138–3146.
- [13] Rivera, P.; Schaibley, J. R.; Jones, A. M.; Ross, J. S.; Wu, S.; Aivazian, G.; Klement, P.; Seyler, K.; Clark, G.; Ghimire, N. J. et al. Observation of long-lived interlayer excitons in monolayer MoSe₂-WSe₂ heterostructures. *Nature Communications* **2015**, *6*, 6242.
- [14] Rigosi, A. F.; Hill, H. M.; Li, Y.; Chernikov, A.; Heinz, T. F. Probing Interlayer Interactions in Transition Metal Dichalcogenide Heterostructures by Optical Spectroscopy: MoS₂/WS₂ and MoSe₂/WSe₂. *Nano Letters* **2015**, *15*, 5033–5038.

- [15] Jauregui, L. A.; Joe, A. Y.; Pistunova, K.; Wild, D. S.; High, A. A.; Zhou, Y.; Scuri, G.; de Greve, K.; Sushko, A.; Yu, C. H. et al. Electrical control of interlayer exciton dynamics in atomically thin heterostructures. *Science* **2019**, *366*, 870–875.
- [16] Ross, J. S.; Rivera, P.; Schaibley, J.; Lee-Wong, E.; Yu, H.; Taniguchi, T.; Watanabe, K.; Yan, J.; Mandrus, D.; Cobden, D. et al. Interlayer Exciton Optoelectronics in a 2D Heterostructure p-n Junction. *Nano Letters* **2017**, *17*, 638–643.
- [17] Liu, Y.; Fang, H.; Rasmita, A.; Zhou, Y.; Li, J.; Yu, T.; Xiong, Q.; Zheludev, N.; Liu, J.; Gao, W. Room temperature nanocavity laser with interlayer excitons in 2D heterostructures. *Science Advances* **2019**, *5*, eaav4506.
- [18] Paik, E. Y.; Zhang, L.; Burg, G. W.; Gogna, R.; Tutuc, E.; Deng, H. Interlayer exciton laser with extended spatial coherence in an atomically-thin heterostructure. *Nature* **2019**, *576*, 80–84.
- [19] Wei, G.; Stanev, T. K.; Czaplowski, D. A.; Jung, I. W.; Stern, N. P. Silicon-nitride photonic circuits interfaced with monolayer MoS₂. *Applied Physics Letters* **2015**, *107*, 091112.
- [20] Ren, T.; Song, P.; Chen, J.; Loh, K. P. Whisper Gallery Modes in Monolayer Tungsten Disulfide-Hexagonal Boron Nitride Optical Cavity. *ACS Photonics* **2018**, *5*, 353–358.
- [21] Kim, S.; Fröch, J. E.; Christian, J.; Straw, M.; Bishop, J.; Totonjian, D.; Watanabe, K.; Taniguchi, T.; Toth, M.; Aharonovich, I. Photonic crystal cavities from hexagonal boron nitride. *Nature Communications* **2018**, *9*, 2623.
- [22] Fröch, J. E.; Hwang, Y.; Kim, S.; Aharonovich, I.; Toth, M. Photonic Nanostructures from Hexagonal Boron Nitride. *Advanced Optical Materials* **2019**, *7*, 1801344.
- [23] Ren, T.; Loh, K. P. On-chip integrated photonic circuits based on two-dimensional materials and hexagonal boron nitride as the optical confinement layer. *Journal of Applied Physics* **2019**, *125*, 230901.
- [24] Lee, G. H.; Cui, X.; Kim, Y. D.; Arefe, G.; Zhang, X.; Lee, C. H.; Ye, F.; Watanabe, K.; Taniguchi, T.; Kim, P. et al. Highly Stable, Dual-Gated MoS₂ Transistors Encapsulated by Hexagonal Boron Nitride with Gate-Controllable Contact, Resistance, and Threshold Voltage. *ACS Nano* **2015**, *9*, 7019–7026.
- [25] Förg, M.; Colombier, L.; Patel, R. K.; Lindlau, J.; Mohite, A. D.; Yamaguchi, H.; Glazov, M. M.; Hunger, D.; Högele, A. Cavity-control of interlayer excitons in van der Waals heterostructures. *Nature Communications* **2019**, *10*, 3697.
- [26] Wang, L.; Meric, I.; Huang, P. Y.; Gao, Q.; Gao, Y.; Tran, H.; Taniguchi, T.; Watanabe, K.; Campos, L. M.; Muller, D. A. et al. One-dimensional electrical contact to a two-dimensional material. *Science* **2013**, *342*, 614–617.
- [27] Zomer, P. J.; Guimarães, M. H.; Brant, J. C.; Tombros, N.; Van Wees, B. J. Fast pick up technique for high quality heterostructures of bilayer graphene and hexagonal boron nitride. *Applied Physics Letters* **2014**, *105*, 013101.
- [28] Ross, J. S.; Wu, S.; Yu, H.; Ghimire, N. J.; Jones, A. M.; Aivazian, G.; Yan, J.; Mandrus, D. G.; Xiao, D.; Yao, W. et al. Electrical control of neutral and charged excitons in a monolayer semiconductor. *Nature Communications* **2013**, *4*, 1474.
- [29] Karni, O.; Barré, E.; Lau, S. C.; Gillen, R.; Ma, E. Y.; Kim, B.; Watanabe, K.; Taniguchi, T.; Maultzsch, J.; Barmak, K. et al. Infrared Interlayer Exciton Emission in MoS₂/WSe₂ Heterostructures. *Physical Review Letters* **2019**, *123*, 247402.
- [30] Zhang, C.; Chuu, C. P.; Ren, X.; Li, M. Y.; Li, L. J.; Jin, C.; Chou, M. Y.; Shih, C. K. Interlayer couplings, Moiré patterns, and 2D electronic superlattices in MoS₂/WSe₂ hetero-bilayers. *Science Advances* **2017**, *3*, e1601459.
- [31] Hsu, C.; Frisenda, R.; Schmidt, R.; Arora, A.; de Vasconcellos, S. M.; Bratschitsch, R.; van der Zant, H. S.; Castellanos-Gomez, A. Thickness-Dependent Refractive Index of 1L, 2L, and 3L MoS₂, MoSe₂, WS₂, and WSe₂. *Advanced Optical Materials* **2019**, *7*, 1900239.
- [32] Binder, J.; Howarth, J.; Withers, F.; Molas, M. R.; Taniguchi, T.; Watanabe, K.; Faugeras, C.; Wysmolek, A.; Danovich, M.; Fal'ko, V. I. et al. Upconverted electroluminescence via Auger scattering of interlayer excitons in van der Waals heterostructures. *Nature Communications* **2019**, *10*, 2335.